Journal of Medicinal Chemistry

Article

pubs.acs.org/jmc

Histone Deacetylase (HDAC) Inhibitors with a Novel Connecting Unit Linker Region Reveal a Selectivity Profile for HDAC4 and HDAC5 with Improved Activity against Chemoresistant Cancer Cells

Linda Marek,[†] Alexandra Hamacher,[†] Finn K. Hansen, Krystina Kuna, Holger Gohlke, Matthias U. Kassack, and Thomas Kurz*

Institut für Pharmazeutische und Medizinische Chemie, Heinrich Heine Universität, Universitätsstrasse 1, 40225 Düsseldorf, Germany

Supporting Information

ABSTRACT: The synthesis and biological evaluation of new potent hydroxamate-based HDAC inhibitors with a novel alkoxyamide connecting unit linker region are described. Biological evaluation includes MTT and cellular HDAC assays on sensitive and chemoresistant cancer cell lines as well as HDAC profiling of selected compounds. Compound **19i** (LMK235) (*N*-((6-(hydroxyamino)-6-oxohexyl)oxy)-3,5-dimethylbenzamide) showed similar effects compared to vorinostat on inhibition of cellular HDACs in a pan-HDAC assay but enhanced cytotoxic effects against the human cancer cell lines A2780, Cal27, Kyse510, and MDA-MB231. Subsequent HDAC profiling yielded a novel HDAC isoform selectivity profile of **19i** in comparison to vorinostat or trichostatin A (TSA). **19i** shows nanomolar inhibition of HDAC4 and HDAC5, whereas vorinostat and TSA inhibit HDAC4 and HDAC5 in the higher micromolar range.

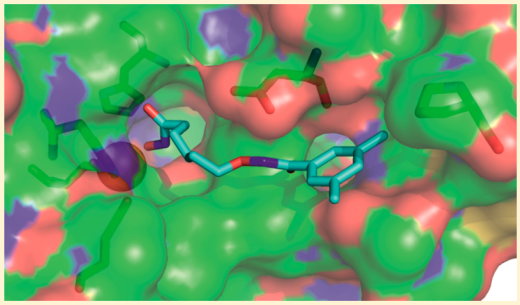

INTRODUCTION

Histone deacetylases (HDACs) play a key role in the epigenetic modulation of gene expression by remodeling chromatin structure.[1] Specifically, HDACs catalyze the removal of acetyl groups from *N*-acetyllysine residues of histones and other cellular proteins (e.g., HSP90, tubulin) during post-translational protein modification.[2] Deacetylation causes chromatin condensation leading mainly to transcriptional suppression, whereas acetylation by histone acetyl transferases (HATs) generally leads to gene activation.[2] HDAC classes I (HDACs 1−3, 8), IIa (HDACs 4, 5, 7, 9), IIb (HDACs 6, 10), and IV (HDAC 11) are Zn^{2+} dependent enzymes, while class III HDACs (sirtuins) are NAD^{+} dependent.[3,4] Class I HDACs are predominantly located in the nucleus, and class II HDACs are in the nucleus and cytoplasm.[3]

HDACs are not only regulators of mitosis, cell differentiation, apoptosis, and chromatin organization but are also involved in the regulation of metabolism, learning, memory, and immune response.[5] As clinically validated cancer targets, their inhibition has been proven to be a successful strategy for the development of novel anticancer drugs.[6] The HDAC inhibitor-induced cell death is mediated through several pathways. Cell growth arrest, differentiation, induction of apoptosis, antiangiogenic effects, and effects on DNA repair and on mitosis have been observed in cancer cells after HDAC inhibition.[5c]

Structurally, HDAC inhibitors are characterized by a cap group connecting unit (CU) linker chelator pharmacophore model.[3] Crystal structures of HDAC-Zn^{2+} inhibitor complexes revealed that the chelator binds to the catalytically important Zn^{2+} ion located at the bottom of the active side.[7] The linker mimics the *N*-acetyllysine side chain within a narrow hydrophobic channel of 11 Å length and connects the chelating group via a connecting unit with a hydrophobic cap group.[3,7a] Linear, aromatic, and cinnamoyl linkers have been often used, while the cap groups are mainly of aromatic or heteroaromatic nature.[3] The cap group interacts with amino acid side chains of the rim region of the active site cavity. Recent results have shown that the nature of the linker, CU, and cap group has an impact on the zinc hydroxamate chelation mode and therefore on the development of subtype selective and/or class selective HDAC inhibitors.[3]

The most promising classes of HDAC inhibitors discovered so far are hydroxamic acids ((trichostatin A (TSA), vorinostat (SAHA), depsipeptides (romidepsin), short-chain fatty acids (valproic acid), and *o*-aminoanilides (mocetinostat and entinostat); Figure 1). Until now, the pan-HDAC inhibitor vorinostat and the class I selective prodrug romidepsin have been approved for treatment of cutaneous T-cell lymphoma (CTCL).[8] In addition, various hydroxamate-based analogues of vorinostat including panobinostat (phase III) and belinostat (phase III) as well as the *o*-aminoanilides (mocetinostat and etinostat, phase II) are under extensive clinical investigations.[5c]

Received: August 31, 2012
Revised: December 18, 2012
Accepted: December 20, 2012
Published: December 20, 2012

dx.doi.org/10.1021/jm301254q | *J. Med. Chem.* 2013, 56, 427−436

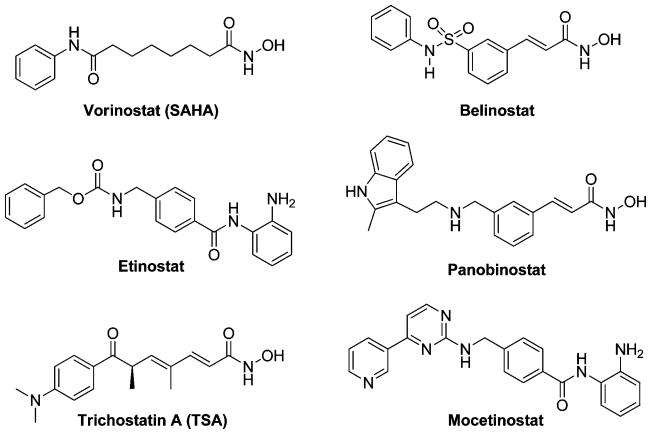

Figure 1. Selected HDAC inhibitors.

First phase I and phase II studies demonstrate that pan-HDAC inhibitors may also cause numerous side effects such as bone marrow depression, diarrhea, weight loss, taste disturbances, electrolyte changes, disordered clotting, fatigue, and cardiac arrhythmias.[9] More recent results suggest that inhibition of specific HDACs might be helpful to discover more effective inhibitors with reduced side effects.[10] However, more data are required to understand if subtype selective, class selective, or broad spectrum inhibitors are to be preferred in cancer treatment. Current clinical data suggest that it depends on the cancer type and the specific drug combination if subtype selective, class selective, or broad spectrum inhibitors are to be preferred in clinical use.[8,11]

Current clinical and preclinical data suggest that HDAC inhibitors have potential for the treatment of several cancer types either alone or in combination with other cytostatic drugs.[12] Notably, the combination of HDAC inhibitors with various established anticancer drugs (e.g., cisplatin) enhanced the cytotoxicity of classical chemotherapeutic agents in hematological and solid tumors.[9,13]

On the basis of a widely accepted HDAC pharmacophore model, we now report on the development and biological evaluation of a new class of potent hydroxamate-based HDAC inhibitors. Cap group, CU, and linker region were modified, and the resulting scaffolds were combined with different ZBGs (Figure 2). The biological evaluation of the target compounds includes MTT assays, pan-HDAC assays on sensitive and chemoresistant cancer cell lines, and in the case of the most active derivatives HDAC profiling with selected HDACs.

RESULTS AND DISCUSSION

Chemistry. Potential HDAC inhibitors with a novel linker region were synthesized as illustrated in Schemes 1−4. The first series of compounds was obtained starting from benzyl 6-((1,3-dioxoisoindolin-2-yl)oxy)hexanoate **3a** or benzyl 6-((1,3-dioxoisoindolin-2-yl)oxy)pentanoate **3b**, which were prepared via O-alkylation of *N*-hydroxyphthalimide **1** with benzyl *ω*-bromocarboxylates **2a**,**b**. Deprotection of the phthaloyl group of **3a**,**b** utilizing methylhydrazine in ethanol provided the O-substituted aminoxy derivatives **4a**,**b**. Subsequently, **4a**,**b** were converted into the alkoxyurea derivatives **5a**−**f** by treatment with isocyanates. The attempted preparation of the alkoxy-amino compound **6a** using benzoyl chloride provided a diacylated byproduct. Consequently, we developed a mild and selective synthesis of **6a** utilizing 1-ethyl-3-(3-dimethylamino-propyl)carbodiimide hydrochloride (EDC) in the presence of a catalytic amount of 4-dimethylaminopyridine (DMAP) as coupling agent, which furnished smoothly the desired intermediate **6a** in 88% yield. In order to obtain the

Scheme 1. Synthesis of Carboxylic Acid Derivatives 8−10[a]

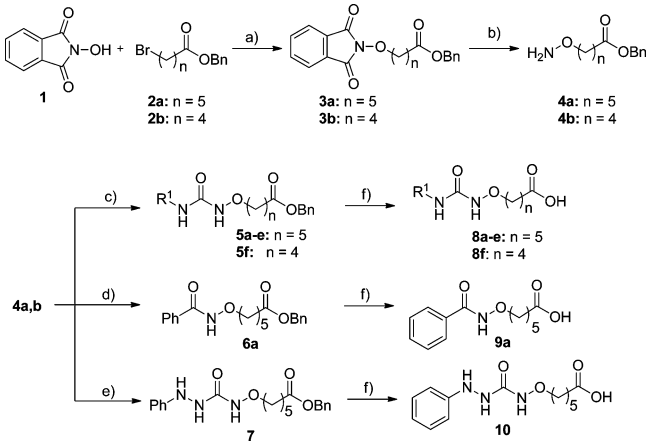

[a]Reagents and conditions: (a) Et_3N, CH_3CN, reflux, 3−5 h; (b) methylhydrazine, CH_2Cl_2, −10 °C, 2 h; (c) R^1NCO, CH_2Cl_2, rt, 18 h; (d) PhCOOH, EDC, DMAP, rt, 24 h; (e) (i) CDT, CH_2Cl_2, rt, 2 h; (ii) phenylhydrazine, Et_3N, rt, 18 h; (f) Pd/C, H_2 (1 bar), THF, rt, 2 h.

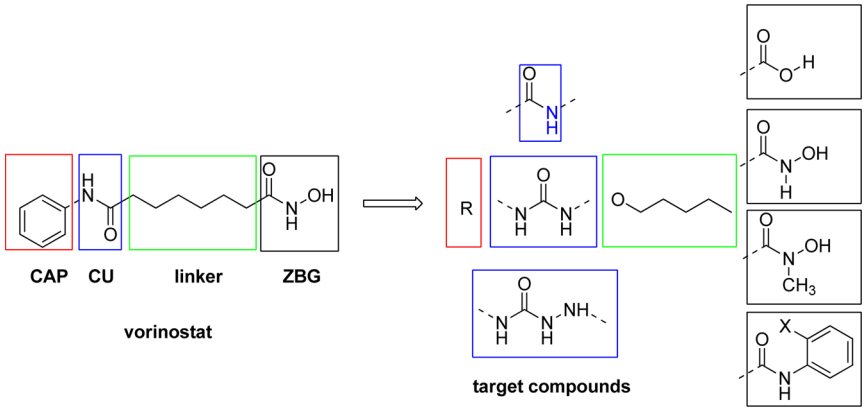

Figure 2. Strategy and target compounds.

dx.doi.org/10.1021/jm301254q | J. Med. Chem. 2013, 56, 427−436

Scheme 2. Synthesis of Target Compounds 16−20[a]

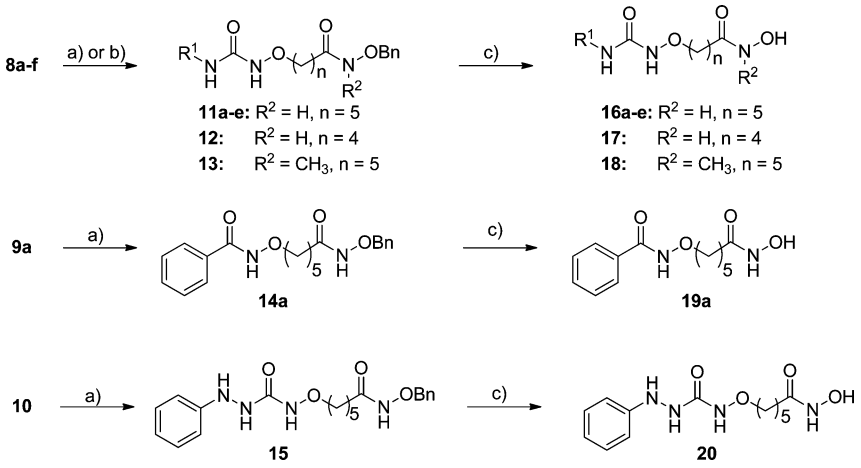

[a]Reagents and conditions: (a) NH_2OBn, EDC, DMAP, rt, 24 h; (b) CH_3NHOBn, EDC, DMAP, rt, 24 h; (c) Pd/C, H_2 (1 bar), THF, rt, 2 h.

alkoxysemicarbazide **7**, compound **4a** was treated with 1,1′-carbonylditriazole (CDT) to give an *N*-triazolide intermediate, which was subsequently reacted with phenylhydrazine to afford alkoxysemicarbazide **7**. The benzyl ester moieties of intermediates **5a−f**, **6a**, and **7** were conveniently deprotected by catalytic hydrogenation to provide the free carboxylic acid derivatives **8a−f**, **9a**, and **10** (Scheme 1).

The preparation of target compounds **16−20** is outlined in Scheme 2. The coupling reactions of **8a−f** with *O*-benzylhydroxylamine utilizing EDC as coupling agent provided the *O*-benzyl protected hydroxamic acids **11a−e** and **12**, which were finally transformed via hydrogenolysis into the desired hydroxamic acid derivatives **16a−e** and chain shortened analogue **17** in yields of 41−67%. The *N*-methyl-substituted hydroxamic acid **18** was obtained from **8a** and *N*-methyl-*O*-benzylhydroxylamine. In a similar fashion, the alkoxyamido derivative **9a** and the semicarbazide **10** were converted into the *O*-benzyl-protected hydroxamic acids **14a** and **15** and subsequently deprotected to yield the target compounds **19a** and **20** in moderate yields (Scheme 2).

In order to efficiently modify the lipophilic cap group while retaining the hydroxamate moiety as ZBG, we developed an improved and straightforward synthetic strategy for compounds of types **16** and **19** utilizing 6-(aminooxy)-*N*-(benzyloxy)-hexanamide **23** as key intermediate (Scheme 3). For this purpose, benzyl 6-((1,3-dioxoisoindolin-2-yl)oxy)hexanoate **3a** was converted into the carboxylic acid **21**. Next, **21** was treated with thionyl chloride to give the corresponding acyl chloride, which was reacted with *O*-benzylhydroxylamine to furnish the *O*-benzyl protected hydroxamic acid **22**. The synthesis of **23** was accomplished by methylhydrazine-mediated cleavage of the phthaloyl protection group. The key intermediate **23** enabled the synthesis of target compounds of types **16** and **19** in a convenient two-step procedure. First, **23** was transformed into the O-protected alkoxyurea derivatives **11f−k** and alkoxyamides **14b−i**. Finally, the catalytic hydrogenation of intermediates **11f−k** and **14b−i** afforded the desired HDAC inhibitors **16f−k** and **19b−i** in yields of 25−94% and 36−86%, respectively.

In order to prepare potential HDAC inhibitors with *o*-amino- and *o*-hydroxyanilide moieties as non-hydroxamate ZGBs, intermediate **21** was transformed into the corresponding acyl chloride. The subsequent reaction with 2-nitroaniline and 2-

Scheme 3. Synthetic Strategy for the Straightforward Modification of the Cap Group[a]

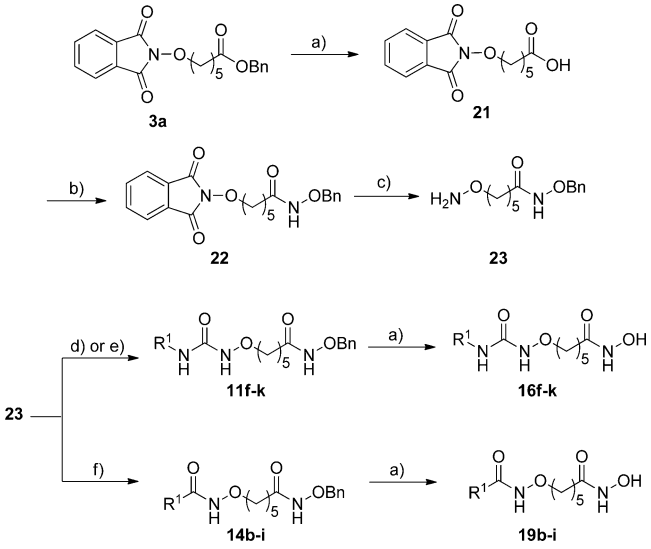

[a]Reagents and conditions: (a) Pd/C, H_2 (1 bar), THF, rt, 2 h; (b) (i) $SOCl_2$, CH_2Cl_2, reflux, 2 h; (ii) NH_2OBn, pyridine, CH_2Cl_2, rt, 18 h; (c) methylhydrazine, CH_2Cl_2, −10 °C, 2 h; (d) R^1NCO, CH_2Cl_2, rt, 18 h; (e) (i) CDT, CH_2Cl_2, rt, 2 h; (ii) R^1NH_2, Et_3N, rt, 18 h; (f) R^1COOH, EDC, DMAP, CH_2Cl_2, rt, 24 h.

benzyloxyaniline generated anilides **24a,b** in overall yields of 82% and 87%, respectively. Cleavage of the phthaloyl protection group and acylation with phenyl isocyanate yielded the *o*-nitro- and *o*-benzyloxyanilides **26** and **27**. Catalytic hydrogenation of **26** afforded the desired *o*-aminoanilide **28** in 46% yield, while deprotection of **27** gave *o*-hydroxyanilide **29** (42% yield, Scheme 4).

Biological Evaluation and Binding Mode. *Cellular Based Activity Assays.* All synthesized target compounds (**8a−29**) were assessed in a MTT assay for cytotoxicity and in a pan-HDAC inhibition assay using the human ovarian cancer cell lines A2780 and its cisplatin resistant subclone A2780CisR. Results are presented in Table 1.

The carboxylic acid derivatives **8a−e** showed weak (**8a**, **8b**) or no (**8c−e**) cytotoxic activity up to 100 μM against both cell lines. Modifications of the lipophilic cap group led to an

dx.doi.org/10.1021/jm301254q | J. Med. Chem. 2013, 56, 427−436

Scheme 4. Synthesis of Target Compounds 28 and 29[a]

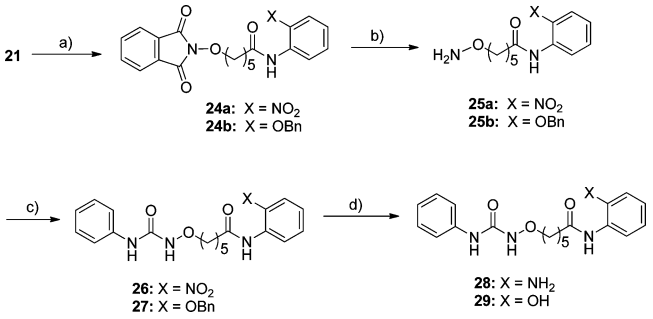

[a]Reagents and conditions: (a) (i) $SOCl_2$, CH_2Cl_2, reflux, 2 h; (ii) 2-nitroaniline or 2-benzyloxyaniline, pyridine, CH_2Cl_2, rt, 18 h; (b) methylhydrazine, CH_2Cl_2, −10 °C, 2 h; (c) phenyl isocyanate, CH_2Cl_2, rt, 18 h; (d) Pd/C, H_2 (1 bar), MeOH, rt, 6 h.

Table 1. Cytotoxic Activity and HDAC Inhibition (IC_{50} [μM]) of 8a−29, Cisplatin, Vorinostat, and TSA against the Human Ovarian Cancer Cell Lines A2780 and A2780 CisR[a]

		cytotoxicity IC_{50} [μM]		HDAC inhibition IC_{50} [μM]	
compd	R^1	A2780	A2780 CisR	A2780	A2780 CisR
8a	Ph	23.5	72.5	>100	>100
8b	4-F-Ph	67.8	73.1	>100	>100
8c	4-CH_3-Ph	>100	>100	nd	nd
8d	4-CH_3O-Ph	>100	>100	nd	nd
8e	1-naphthyl	>100	>100	nd	nd
16a	Ph	8.47	5.47	1.70	1.71
16b	4-F-Ph	9.05	9.34	2.04	1.66
16c	4-CH_3-Ph	8.05	10.2	1.45	1.43
16d	4-CH_3O-Ph	10.3	18.2	6.64	5.73
16e	1-naphthyl	7.63	7.87	1.06	0.90
16f	3-chinolyl	10.8	11.6	1.07	0.85
16g	4-*i*-Pr-Ph	27.1	58.8	2.86	2.05
16h	4-*t*-Bu-Ph	6.34	8.80	1.41	1.32
16i	2-CH_3-Ph	23.0	30.1	11.7	8.86
16j	3-CH_3-Ph	8.33	8.12	7.63	5.38
16k	3,5-CH_3-Ph	2.43	5.11	5.27	4.64
17	Ph	62.6	35.2	15.2	16.6
18	Ph	87.9	>100	>100	>100
19a	Ph	8.33	5.72	1.58	1.26
19b	4-F-Ph	16.4	60.3	2.57	2.00
19c	4-CF_3-Ph	9.53	30.8	2.09	1.95
19d	4-*i*-Pr-Ph	4.13	4.96	0.60	0.50
19e	3-CH_3-Ph	2.10	2.25	1.58	0.90
19f	4-CH_3-Ph	4.09	5.00	4.21	3.46
19g	2-CH_3-Ph	25.6	33.8	17.1	15.4
19h	3,4-CH_3-Ph	1.54	1.78	1.61	0.88
19i	3,5-CH_3-Ph	0.49	0.32	0.65	0.32
20	Ph	34.9	42.4	5.86	4.95
28		62.5	86.9	34.0	43.9
29		35.0	84.6	34.0	43.9
cisplatin		1.56	13.4	ne	ne
vorinostat		2.42	3.12	0.53	0.44
TSA		0.29	0.22	0.43	0.25

[a]nd = not determined. ne = no effect up to 316 μM. Values are the mean of three experiments. The standard deviations are <10% of the mean.

increase in cytotoxic activity. The majority of the compounds showed IC_{50} values in the micromolar range. The most active compound of this series, **19i**, gave IC_{50} values of 0.49 μM (A2780) and 0.32 μM (A2780 CisR), which was even lower than those of the reference compound vorinostat or the cytotoxic agent cisplatin. For the majority of compounds, the cytotoxic activity was similar at the parental and cisplatin resistant subclone.

The carboxylic acid derivatives displayed no inhibitory activity in the cellular pan-HDAC assay up to 100 μM. Most probably, this lack of activity is attributed to the weaker zinc binding properties of the carboxyl group in comparison to the hydroxamate moiety. Since **8c−e** were inactive in the MTT assay up to 100 μM, their inhibitory activity in the pan-HDAC assay was not determined in this study. All other compounds with the exception of **18** showed IC_{50} values for HDAC inhibition in the micromolar range which were similar to their cytotoxic activity.

Differences between HDAC inhibition and cytotoxicity values may be attributed to differences in incubation times used in these assays. However, we do see a significant correlation between HDAC inhibition and MTT data, which supports, but does not prove, the hypothesis that HDAC inhibition mediates cytotoxicity (Figure S1 of Supporting Information).

Important structural requirements for potent HDAC inhibition are a hydroxamic acid ZBG, a connecting unit linker region and a hydrophobic dimethyl substituted phenyl ring as a suitable CAP group. The most potent compounds in the cellular HDAC assay were **19d** and **19i** showing IC_{50} values of 0.60/0.50 and 0.65/0.32 μM, respectively, which is about equipotent to the reference compounds vorinostat and TSA.

In consideration of cytotoxic and HDAC inhibition activity, **19e**, **19h**, and **19i** were the most active compounds of this series. Interestingly, all three compounds showed a comparable cytotoxic activity at A2780 and its cisplatin resistant subclone A2780 CisR with a slightly higher pan-HDAC inhibition at A2780 CisR (**19e**, 1.20-fold; **19h**, 1.83-fold; **19i**, 2.03-fold). This effect was similar for TSA and vorinostat. To further investigate the activity of **19e**, **19h**, and **19i** in chemoresistant cell lines, the cytotoxicity and HDAC inhibitory activities of **19e**, **19h**, and **19i** were tested at the human triple negative breast cancer cell line MDA-MB-231, the human tongue cancer cell line Cal27, the human esophagus cell line Kyse510, and their cisplatin resistant subclones. The results are shown in Table 2. **19e**, **19h**, **19i**, and vorinostat showed similar inhibition in the parental and the cisplatin-resistant subclones in MTT and HDAC assays except for a 2.3- to 2.8-fold higher HDAC inhibition in Kyse510 CisR compared to Kyse sens. However, the slightly higher inhibition of HDAC in Kyse CisR is not leading to a higher cytotoxicity in Kyse CisR. Again, **19i** was the most potent compound and displayed a higher cytotoxicity and HDAC inhibitory activity than the reference compound vorinostat.

HDAC IC_{50} Profiling. The three most cytotoxic compounds **19e**, **19h**, and **19i** were selected for a HDAC profiling against seven HDAC isoforms (1, 2, 4, 5, 6, 8, and 11). Vorinostat and TSA were used as reference compounds (Table 3).

The isoform assays show that compounds **19e**, **19h**, and **19i** display a profile against HDACs 1, 2, 8, 11 similar to vorinostat. However, **19e**, **19h**, and **19i** showed increased inhibitory activity at HDACs 4, 5, and 6. **19h** displayed the highest activity at HDAC6 with an IC_{50} of 18.1 nM, whereas **19e** and **19i** showed selectivity for HDAC isoforms 4 and 5. **19i** exhibited the highest activity on HDAC4 with an IC_{50} of 11.9 nM. **19e**

dx.doi.org/10.1021/jm301254q | J. Med. Chem. 2013, 56, 427−436

Table 2. Cytotoxicity (MTT Assay) (A) and HDAC Inhibition Activity (B) of 19e, 19h, 19i, Cisplatin, and Vorinostat against Human Cancer Cell Lines with Different Sensitivity Towards Cisplatin[a]

	(A) MTT Assay IC_{50} [μM] of cell line					
	MDA-MB-231		Cal27		Kyse510	
compd	sens	CisR	sens	CisR	sens	CisR
19e	2.79	3.81	2.97	3.72	8.19	8.21
19h	2.77	3.77	2.90	4.31	10.0	9.46
19i	1.37	1.68	1.03	1.81	2.96	2.48
vorinostat	1.66	2.69	2.64	2.08	4.62	4.66
cisplatin	35.7	96.5	19.2	43.9	2.49	8.44
	(B) HDAC Assay IC_{50} [μM] of cell line					
	MDA-MB-231		Cal27		Kyse510	
compd	sens	CisR	sens	CisR	sens	CisR
19e	1.41	1.28	1.00	0.88	2.62	1.13
19h	1.57	1.66	1.10	0.91	2.82	1.10
19i	0.46	0.41	0.36	0.36	1.00	0.35
vorinostat	0.61	0.61	0.36	0.61	0.70	0.59
cisplatin	ne	ne	ne	ne	ne	ne

[a]ne = no effect up to a concentration of 316 μM. Data are IC_{50} values in μM. Values are the mean of three experiments. The standard deviations are <10% of the mean.

showed the highest activity on HDAC5 with an IC_{50} of 2.31 nM. **19e** and **19i** showed a 11- to 13-fold selectivity for HDAC5 over HDAC6.

*Binding Mode of **19i** in HDAC4 and HDAC8.* In order to understand differences in the inhibition activities of compounds **19e**, **19h**, and **19i** with respect to HDAC4 and HDAC8, **19i**, which shows the highest selectivity for HDAC4 over HDAC8, was docked into the crystal structures of HDAC4 (PDB code 2VQW) and HDAC8 (PDB code 2V5W) using AutoDock3[14] as a docking engine and DrugScore[15] as an objective function. Both HDAC structures have a "closed" conformation of the structural zinc-binding domain[16] and have been used successfully for docking previously.[17] For evaluating the applied docking approach, we initially performed cross-docking of the hydroxamic acid ligands taken from PDB code 2VQM (HDAC4) (1W22 (HDAC8)) to the structure of 2VQW (2V5W). Despite the fact that cross-docking is a more stringent test than re-docking,[18] in both cases good docking solutions (root-mean-square deviation of the ligand atoms after superimposing the respective protein structures was 2.71 Å (2.42 Å)) were identified in the second largest (largest) cluster, validating the combination AutoDock3/DrugScore as a suitable docking approach.

When **19i** was docked, the compound showed more favorable interactions with the catalytic zinc ion of HDAC4 than of HDAC8, as demonstrated by distances between the oxygen of the hydroxy group of the hydroxamic acid and the zinc ion of <2 Å (<3 Å) found in 6% (31%) of the dockings to HDAC4 and in 0% (4%) of the dockings to HDAC8. These differences arise from differences in the binding modes of the ligand (Figure 3). In the case of HDAC4, **19i** orients its phenyl

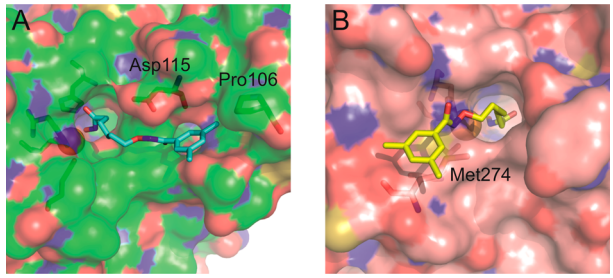

Figure 3. Binding mode of **19i** in HDAC4 (A, PDB code 2VQW) and HDAC8 (B, PDB code 2V5W) as predicted by docking. Amino acids discussed in the text are labeled and shown in stick representation. The zinc ion is shown as orange sphere, and the residues coordinating it are in stick representation.

moiety into a groove formed by loop $\alpha1-\alpha2$, loop $\beta4-\alpha8$, and loop $\beta5-\alpha9$. In the case of HDAC8, **19i** orients this moiety into a shallow indentation formed by loop $\beta7-\beta8$ and loop $\beta9-\alpha15$. The respective other binding region is sterically occupied in both cases.

These differences in the binding modes provide an explanation for the observed selectivity of **19i** (Figure 3). In HDAC4, a charge-assisted hydrogen bond between the alkoxyamide nitrogen and the carboxylate group of Asp115 is formed (O–N distance, 2.6 Å), which presumably is enforced by the additional polarization of the N–H bond due to the presence of the *N*-alkoxy moiety. In contrast, in HDAC8, a hydrogen bond is formed between the alkoxyamide nitrogen and the sulfur atom of Met274 (S–N distance, 3.5 Å). The latter is a much weaker hydrogen bond acceptor than the carboxylate group. These findings suggest that the novel alkoxyamide connecting unit linker region contributes to the selectivity of **19i**. The binding mode in HDAC4 also explains why the inhibition activity of **19h** against this isoform is lower by factors of ~5 and ~8 than those of **19e** and **19i** (Table 3). In the case of **19h**, the 4-methyl group at the phenyl ring would sterically interfere with Pro106, which would lead to a shift of the alkoxyamide moiety and, hence, likely to a breaking of the charge-assisted hydrogen bond with Asp115. In contrast, **19e** and **19i** show a similar inhibition activity against HDAC4, which is in agreement with the fact that one of the two methyl

Table 3. Inhibition Activities (IC_{50} [nM]) of Compounds 19e, 19h, 19i, Vorinostat, and TSA against HDAC Isoforms 1, 2, 4, 5, 6, 8, and 11

	IC_{50} [nM] of HDAC isoforms						
compd	1	2	4	5	6	8	11
19e	341	1392	16.3	2.31	26.9	1043	2135
19h	320	944	82.6	33.4	18.1	833	997
19i	320	881	11.9	4.22	55.7	1278	852
vorinostat	320	920	48300	20000	160	960	480
TSA	10.9	32.1	8439	6155	1.50	196	31.0

dx.doi.org/10.1021/jm301254q | *J. Med. Chem.* 2013, 56, 427–436

groups of **19i** is oriented toward the solvent; hence, removing it, as done in **19e**, has a small effect only on the inhibition activity. In contrast, because of the more solvent-exposed binding mode of **19i** in HDAC8, neither removing the second methyl group (**19e**) nor shifting one group into the 4-position (**19h**) is expected to have a profound effect on the inhibition activity, in line with observed differences of a factor of <1.6 (Table 3).

In summary, docking studies suggest distinct binding modes of **19i** in HDAC4 and HDAC8. These binding modes are in line with and provide structural explanations for the observed selectivity of **19i** for HDAC4 over HDAC8 as well as the differences in the inhibition activities of **19e**, **19h**, and **19i** with respect to HDAC4 and HDAC8, respectively.

*Enhancement of Cisplatin-Induced Toxicity by **19i**.* Vorinostat and **19i** alone showed a concentration-dependent cytotoxic effect on different cancer cell lines (Table 1 and Table 2A). On the basis of their potent cytotoxic and HDAC inhibitory activity, we investigated a possible enhancement of the cytotoxic effect of cisplatin in combination with **19i** in four different cisplatin resistant cell lines (Cal27 CisR, A2780 CisR, Kyse510 CisR, and MDA-MB231 CisR). Vorinostat was used as reference compound. The cell lines were pretreated with vorinostat or **19i** for 48 h followed by a treatment with cisplatin for 72 h.

The combination of cisplatin and vorinostat or **19i** markedly enhanced the sensitivity of platinum-resistant cell lines to cisplatin (Table 4). IC_{50} values for cisplatin in combination with vorinostat or **19i** (Table 4) were even lower than IC_{50} values for the corresponding parental cell lines (Table 2A). The combination of cisplatin and **19i** was more effective than the cisplatin−vorinostat combination, as can be seen from higher shift factors (SF) for the cisplatin/**19i** combination (Table 4). A remarkably high chemosensitization against cisplatin was observed for the HNSCC cell lines Cal27 CisR and Kyse510 CisR with shift factors of 21.6 and 18.8, respectively. Furthermore, the combination of cisplatin and **19i** produced a higher reduction in cell viability in comparison to the combination of cisplatin and vorinostat in all cell lines. Accordingly, **19i** is a novel nanomolar HDAC inhibitor that reverts cisplatin resistance in different human cancer cell lines.

In order to gather additional information about the interaction between cisplatin and **19i** as well as between cisplatin and vorinostat, concentration−effect analyses were performed (Table 5). The concentrations of **19i** and vorinostat used were 0.25, 0.5, 1.0, and 1.5 μM for all cell lines, while the concentrations of cisplatin were selected for each tumor cell line from the cisplatin-induced growth inhibition curve. The highest cisplatin concentration represents the IC_{50} value, whereas the other four used concentrations were below the IC_{50} values of cisplatin.

19i and vorinostat enhanced in a concentration-dependent manner the cytotoxic effect of cisplatin. The combination index analysis based on the Chou−Talalay method revealed a synergistic interaction with cisplatin (CI < 0.9) for both compounds. All four cisplatin-resistant tumor cell lines showed higher synergistic effects (=lower CIs) for the combination of cisplatin and **19i** in comparison to the cisplatin vorinostat combination, except for 1.5 μM vorinostat in A2780 CisR.

Especially in the cisplatin-resistant HNSCC cell lines Cal27 CisR and Kyse510, **19i** enhanced markedly the cytotoxicity of cisplatin. The CI for **19i** in Kyse510 CisR is less than 0.2, which

Table 4. IC_{50} [μM] of Cisplatin in Cisplatin Resistant A2780 CisR, Cal27 CisR, Kyse510 CisR, and MDA-MB231 CisR Cell Lines after Treatment with Cisplatin or in Combination with 1 μM Vorinostat or 1 μM 19i[a]

		cisplatin + vorinostat		cisplatin + **19i**	
cell line	cisplatin, IC_{50}	IC_{50}	SF	IC_{50}	SF
A2780 CisR	13.4	5.80	2.31	3.33	4.02
Cal27 CisR	43.9	2.53	17.4	2.03	21.6
Kyse510 CisR	8.44	0.78	10.8	0.45	18.8
MDA-MB231 CisR	96.5	65.8	1.47	27.3	3.53

[a]SF means shift factor and was calculated by dividing the IC_{50} of cisplatin alone by the IC_{50} of the corresponding drug combination. Values are the mean of three experiments. The standard deviations are <10% of the mean.

Table 5. Synergism Studies between Cisplatin and 19i and Vorinostat[a]

	19i [μM]				vorinostat [μM]			
(A) MDA-MB-231 CisR								
cisplatin	0.25	0.5	1	1.5	0.25	0.5	1	1.5
5	*	*	*	0.82	*	*	*	*
10	*	*	0.85	0.79	*	*	*	*
25	*	0.79	0.72	0.73	*	*	0.88	0.83
40	*	0.88	0.78	0.84	*	*	1.00	0.91
50	0.90	0.81	0.75	0.80	0.92	0.93	0.84	0.88
(B) Cal27 CisR								
	19i [μM]				vorinostat [μM]			
cisplatin	0.25	0.5	1	1.5	0.25	0.5	1	1.5
1	*	*	*	0.48	*	*	*	*
2.5	*	*	0.38	0.34	*	*	*	0.93
5	*	0.45	0.26	0.22	*	*	0.65	0.37
10	0.85	0.41	0.24	0.20	*	*	0.53	0.30
45	0.27	0.31	0.27	0.23	0.39	0.38	0.29	0.31
(C) Kyse510 CisR								
	19i [μM]				vorinostat [μM]			
cisplatin	0.25	0.5	1	1.5	0.25	0.5	1	1.5
0.5	0.18	0.13	0.08	0.06	0.71	0.52	0.66	0.75
0.75	0.10	0.07	0.05	0.05	0.51	0.44	0.67	0.68
1	0.13	0.08	0.05	0.05	0.47	0.42	0.56	0.60
3.16	0.18	0.09	0.09	0.12	0.46	0.50	0.55	0.51
8	0.18	0.16	0.18	0.16	0.24	0.23	0.27	0.42
(D) A2780 CisR								
	19i [μM]				vorinostat [μM]			
cisplatin	0.25	0.5	1	1.5	0.25	0.5	1	1.5
1	*	0.85	0.82	0.97	*	*	0.86	0.86
5	0.85	0.73	0.64	0.81	*	0.91	0.74	0.73
8	0.78	0.66	0.59	0.74	*	0.79	0.74	0.69
10	0.78	0.69	0.61	0.68	*	0.72	0.77	0.67
20	0.76	0.58	0.49	0.64	0.79	0.68	0.62	0.56

[a]The cisplatin-resistant tumor cell lines MDA-MB-231 (A), Cal27 CisR (B), Kyse510 CisR (C), and A2780 CisR (D) were treated with different combinations of cisplatin and **19i**/vorinostat. CI (combination index) was calculated using CalcuSyn 2.1 based on the Chou−Talalay method. CI > 1.0 indicates antagonism. CI = 1 indicates an additive effect, and CI < 0.9 indicates synergism. * = fraction affected less than 0.20. Values are the mean of three experiments. Standard deviation is <10% of the mean.

dx.doi.org/10.1021/jm301254q | J. Med. Chem. 2013, 56, 427−436

indicates a very strong synergism, whereas the CI for vorinostat indicates a moderate synergism. This is in accordance with the observed higher shift factors for **19i** in HNSCC in comparison to vorinostat (Table 4). The synergistic effect of **19i** was not only observed for the combination with cisplatin in a concentration of 1 μM (a concentration near the IC_{50} of **19i**), it was also detected for lower concentrations (0.25 and 0.5 μM). Even in combinations of **19i** with low-dose cisplatin a highly synergistic interaction was detected. On the basis of the results, we draw the conclusion that **19i** acts with cisplatin in a synergistic manner and enhances the cytotoxicity of cisplatin to a greater extent than vorinostat, especially in HNSCC cell lines.

CONCLUSION

On the basis of a widely accepted HDAC pharmacophore model, we developed new potent hydroxamate-based HDAC inhibitors with a novel alkoxyamide connecting unit linker region. Their cytotoxicity and HDAC inhibitory activity were determined in different human cisplatin sensitive and resistant cancer cell lines by MTT and HDAC inhibition assays. **19i** (LMK235) (*N*-((6-(hydroxyamino)-6-oxohexyl)oxy)-3,5-dimethylbenzamide) was identified as the most cytotoxic compound and displayed equipotent HDAC inhibition in the pan-HDAC assay compared to vorinostat. In contrast to vorinostat, **19i** showed a novel HDAC isoform selectivity profile with preference for HDAC4 and HDAC5, which are inhibited with low nanomolar IC_{50} values. A binding mode of **19i** in HDAC4 predicted by docking provides structural explanations for the observed selectivity of **19i** for HDAC4. The enhanced cytotoxicity of **19i** in the investigated cancer cell lines may be related to this novel selectivity profile. The combination of **19i** with cisplatin enhanced markedly the cisplatin sensitivity of our cisplatin resistant sublines. Pretreatment with **19i** 48 h prior to cisplatin led to a complete resensitization of the platinum resistant cancer cell lines. Most notably, the combination of cisplatin and **19i** was more effective than the cisplatin vorinostat combination. Therefore, it can be assumed that HDAC4 and HDAC5 inhibition may contribute to this chemosensitizing effect of **19i**. Our findings are in agreement with recent results of Stronach et al. who showed that silencing of HDAC4 led to an increase in cisplatin sensitivity.[19] We believe that especially compound **19i** is a promising starting point for further structural optimization. As a class IIa selective HDAC inhibitor, **19i** could be a promising tool to investigate the function of these isoforms concerning the molecular mechanism of cancer development and treatment.

EXPERIMENTAL SECTION

1. Chemistry. General. All solvents and chemicals were used as purchased without further purification. The progress of all reactions was monitored on Merck precoated silica gel plates (with fluorescence indicator UV_{254}) using ethyl acetate/*n*-hexane as solvent system. Column chromatography was performed with Fluka silica gel 60 (230−400 mesh ASTM) with the solvent mixtures specified in the corresponding experiment. Spots were visualized by irradiation with ultraviolet light (254 nm). Melting points were taken in open capillaries on a Mettler FP 5 melting point apparatus and are uncorrected. Proton (^{1}H) and carbon (^{13}C) NMR spectra were recorded on a Bruker Avance 500 (500.13 MHz for ^{1}H; 125.76 MHz for ^{13}C) using DMSO-d_6 and $CDCl_3$ as solvents. Chemical shifts are given in parts per million (ppm) (δ relative to residual solvent peak for ^{1}H and ^{13}C and to external tetramethylsilane). Elemental analysis was performed on a Perkin Elmer PE 2400 CHN elemental analyzer. IR spectra were recorded on a Varian 800 FT-IR Scimitar series. HRMS analysis was performed on a UHR-TOF maXis 4G, Bruker Daltonics, Bremen instrument. If necessary, the purity was determined by HPLC: instrument, Elite LaChrom system [Hitachi L-2130 (pump) and L-2400 (UV detector)]; column, Phenomenex Luna C-18(2) 1.8 μm particle (250 mm × 4.6 mm), supported by Phenomenex Security Guard cartridge kit C18 (4.0 mm × 3.0 mm). The purity of all final compounds determined by HPLC was 95% or higher. Compounds **2a,b** and **21** have been prepared according to known procedures.[20]

Experimental Data. General procedures for the synthesis of HDAC inhibitors and compound characterization data for selected compounds **16c**, **17**, **18**, **19i**, **20**, **28**, and **29** are given below. The synthesis of all other compounds is reported in the Supporting Information.

Synthesis of HDAC Inhibitors. General Procedure for the Preparation of Target Compounds 16a−k, 17, 18, 19a−i, 20, 28, and 29. A solution of the respective *O*-benzyl-protected hydroxamic acid or anilide intermediate (2 mmol) in dry THF (150 mL) or methanol (150 mL, in the cases of compounds **28** and **29**) was hydrogenated (1 bar) at room temperature in the presence of a catalytic amount of Pd−C (10 wt %). Upon completion, the crude mixture was filtered through Celite to remove the catalyst and the filtrate was concentrated under reduced pressure. The residue crystallized upon storage in a freezer. The residue was purified by column chromatography using ethyl acetate or ethyl acetate/methanol (9:1) as eluent.

***N*-Hydroxy-6-((3-(*p*-tolyl)ureido)oxy)hexanamide (16c).** Reaction time: 12 h. White solid; yield 67%; mp 121 °C. ^{1}H NMR (500.13 MHz, DMSO-d_6): δ = 1.26−1.35 (m, 2H), 1.46−1.65 (m, 4H), 1.96 (t, J = 7.3 Hz, 2H), 2.24 (s, 3H), 3.74 (t, J = 6.7 Hz, 2H), 7.06 (d, J' = 8.3 Hz, 2H), 7.43 (d, J = 8.3 Hz, 2H), 8.56 (s, 1H), 8.70 (s, 1H), 9.36 (s, 1H), 10.35 (s, 1H) ppm. ^{13}C NMR (125.76 MHz, DMSO-d_6): δ = 20.25, 24.83, 27.15, 32.09, 75.54, 119.54, 128.74, 136.30, 157.06, 168.92 ppm. IR (KBr): $\tilde{\nu}$ = 3323, 3208 (NH), 2937, 2869 (CH_2), 1659 (C═O) cm^{-1}. Anal. Calcd for $C_{14}H_{21}N_3O_4$: C 56.94, H 7.17, N 14.23. Found: C 57.00, H 7.35, N 13.95.

***N*-Hydroxy-5-((3-phenylureido)oxy)pentanamide (17).** Reaction time: 4 h. White solid; yield 41%; mp 83 °C. ^{1}H NMR (500.13 MHz, DMSO-d_6): δ = 1.51−1.68 (m, 4H), 1.99 (t, J = 6.7 Hz, 2H), 3.76 (t, J = 5.9 Hz, 2H), 6.99 (t, J = 7.3 Hz, 1H), 7.26 (t, J = 7.8 Hz, 2H), 7.56 (d, J = 7.8 Hz, 2H), 8.69 (s, 1H), 8.70 (s, 1H), 9.43 (s, 1H), 10.37 (s, 1H) ppm. ^{13}C NMR (125.76 MHz, DMSO-d_6): δ = 21.36, 26.96, 31.85, 75.30, 119.45, 122.32, 128.33, 138.91, 157.01, 168.84 ppm. IR (KBr): $\tilde{\nu}$ = 3214 (NH), 2924, 2877 (CH_2), 1662 (C═O) cm^{-1}. Anal. Calcd for $C_{12}H_{17}N_3O_4$: C 53.92, H 6.41, N 15.72. Found: C 53.72, H 6.69, N 15.42.

***N*-Hydroxy-*N*-methyl-6-((3-phenylureido)oxy)hexanamide (18).** Reaction time: 4 h. White solid; yield 63%; mp 93 °C. ^{1}H NMR (500.13 MHz, DMSO-d_6): δ = 1.28−1.41 (m, 2H), 1.46−1.57 (m, 2H), 1.58−1.68 (m, 2H), 2.35 (t, J = 7.1 Hz, 2H), 3.08 (s, 3H), 3.76 (t, J = 6.7 Hz, 2H), 6.95−7.03 (m, 1H), 7.26 (t, J = 7.9 Hz, 2H), 7.54−7.59 (m, 2H), 8.66 (s, 1H), 9.43 (s, 1H), 9.76 (s, 1H) ppm. ^{13}C NMR (125.76 MHz, DMSO-d_6): δ = 23.96, 25.03, 27.27, 31.34, 35.60, 75.63, 119.47, 122.33, 128.34, 138.91, 157.00, 172.77 ppm. IR (KBr): $\tilde{\nu}$ = 3222 (NH), 2934, 2865 (CH_2), 1660 (C═O) cm^{-1}. Anal. Calcd for $C_{14}H_{21}N_3O_4$: C 56.94, H 7.17, N 14.23. Found: C 56.79, H 7.29, N 14.02.

***N*-((6-(Hydroxyamino)-6-oxohexyl)oxy)-3,5-dimethylbenzamide (19i).** Reaction time: 4 h. Purple solid; yield 58%; mp 132 °C. ^{1}H NMR (500.13 MHz, DMSO-d_6): δ = 1.29−1.39 (m, 2H), 1.48−1.64 (m, 4H), 1.96 (t, J = 7.3 Hz, 2H), 2.30 (s, 6H), 3.84 (t, J = 6.4 Hz, 2H), 7.17 (s, 1H), 7.35 (s, 2H), 8.67 (s, 1H), 10.35 (s, 1H), 11.50 (s, 1H) ppm. ^{13}C NMR (125.76 MHz, DMSO-d_6): δ = 20.70, 24.81, 24.98, 27.34, 32.10, 74.94, 124.66, 132.36, 132.62, 137.44, 164.37, 168.92 ppm. IR (KBr): $\tilde{\nu}$ = 3204 (NH), 2941, 2866 (CH_2), 1671, 1625 (C═O) cm^{-1}. Anal. Calcd for $C_{15}H_{22}N_2O_4$: C 61.21, H 7.53, N 9.52. Found: C 61.47, H 7.71, N 9.73.

***N*-((6-(Hydroxyamino)-6-oxohexyl)oxy)-2-phenylhydrazinecarboxamide (20).** Reaction time: 6 h. Yellow solid; yield 12%; mp 100 °C. ^{1}H NMR (500.13 MHz, DMSO-d_6): δ = 1.24−1.34 (m, 2H), 1.46−1.65 (m, 4H), 1.95 (t, J = 7.3 Hz, 2H), 3.72 (t, J = 6.6 Hz, 2H),

dx.doi.org/10.1021/jm301254q | J. Med. Chem. 2013, 56, 427−436

6.65−6.73 (m, 3H), 7.13 (t, J = 7.7 Hz, 2H), 7.47 (s, 1H), 8.60 (s, 1H), 8.66 (s, 1H), 9.38 (s, 1H), 10.34 (s, 1H) ppm. ^{13}C NMR (125.76 MHz, DMSO-d_6): δ = 24.84, 24.88, 27.20, 32.10, 75.46, 111.91, 118.14, 128.50, 149.77, 159.70, 168.95 ppm. IR (KBr): $\tilde{\nu}$ = 3237 (NH), 2937, 2866 (CH_2), 1658 (C═O) cm^{-1}. Anal. Calcd for $C_{13}H_{20}N_4O_4$: C 52.69, H 6.80, N 18.91. Found: C 52.49, H 7.04, N 18.76.

***N*-(2-Aminophenyl)-6-((3-phenylureido)oxy)hexanamide (28).** Reaction time: 6 h. Yellow solid; yield 46%; mp 128 °C. ^{1}H NMR (500.13 MHz, DMSO-d_6): δ = 1.35−1.44 (m, 2H), 1.58−1.72 (m, 4H), 2.33 (t, J = 7.4 Hz, 2H), 3.79 (t, J = 6.6 Hz, 2H), 4.82 (s, 2H), 6.51−6.56 (m, 1H), 6.71 (d, J = 7.9 Hz, 1H), 6.86−6.92 (m, 1H), 6.98 (t, J = 7.4 Hz, 1H), 7.16 (d, J = 7.8, 1H), 7.25 (t, J = 7.9 Hz, 2H), 7.56 (d, J = 8.2 Hz, 2H), 8.67 (s, 1H), 9.11 (s, 1H), 9.45 (s, 1H) ppm. ^{13}C NMR (125.76 MHz, DMSO-d_6): δ = 24.92, 25.01, 27.23, 35.58, 75.62, 115.77, 116.05, 119.44, 122.21, 123.44, 125.18, 125.58, 128.33, 138.91, 141.77, 156.99, 170.96 ppm. IR (KBr): $\tilde{\nu}$ = 3331, 3223 (NH), 2939, 2864 (CH_2), 1658 (C═O) cm^{-1}. Anal. Calcd for $C_{19}H_{24}N_4O_3$: C 64.03, H 6.79, N 15.72. Found: C 63.96, H 6.69, N 15.82.

***N*-(2-Hydroxyphenyl)-6-((3-phenylureido)oxy)hexanamide (29).** Reaction time: 6 h. White solid; yield 42%; mp 80 °C. ^{1}H NMR (500.13 MHz, DMSO-d_6): δ = 1.29−1.43 (m, 2H), 1.56−1.74 (m, 4H), 2.41 (t, J = 7.3 Hz, 2H), 3.78 (t, J = 6.6 Hz, 2H), 6.75 (t, J = 7.6 Hz, 1H), 6.85 (d, J = 7.9 Hz, 1H), 6.90−7.01 (m, 2H), 7.25 (t, J = 7.9 Hz, 2H), 7.56 (d, J = 8.2 Hz, 2H), 7.68 (d, J = 7.8 Hz, 1H), 8.66 (s, 1H), 9.25 (s, 1H), 9.44 (s, 1H), 9.74 (s, 1H) ppm. ^{13}C NMR (125.76 MHz, DMSO-d_6): δ = 24.89, 24.98, 27.22, 35.73, 75.62, 115.81, 118.86, 119.44, 122.22, 122.32, 124.49, 126.29, 128.33, 138.90, 147.74, 156.99, 171.73 ppm. IR (KBr): $\tilde{\nu}$ = 3349, 3176 (NH), 2951, 2862 (CH_2), 1661 (C═O) cm^{-1}. Anal. Calcd for $C_{19}H_{23}N_3O_4$: C 63.85, H 6.49, N 11.76. Found: C 63.70, H 6.61, N 11.75.

2. Biological Evaluation. Reagents. Trichostatin A and cisplatin were purchased from Invivogen (France) and Sigma (Germany). Vorinostat was synthesized according to known procedures.[21] All other reagents were supplied by PAN Biotech (Germany) unless otherwise stated.

Cell Lines and Cell Culture. The human ovarian carcinoma cell line A2780 was obtained from European Collection of Cell Cultures (ECACC, Salisbury, U.K.). The human tongue cell line Cal27 and the human esophagus cell line Kyse510 were obtained from the German Collection of Microorganisms and Cell Cultures (DSMZ, Germany). The human triple negative breast cancer cell line MDA-MB-231 was obtained from American Type Culture Collection (ATCC, U.S.). The cisplatin resistant CisR cell lines were generated by exposing the parental cell lines to weekly cycles of cisplatin in a IC_{50} concentration over a period of 24−30 weeks as described by Gosepath et al.[22] and Eckstein et al.[23]

All cancer cell lines were grown at 37 °C under humidified air supplemented with 5% CO_2 in RPMI 1640 (A2780, Kyse510) or DMEM (Cal27, MDA-MB-231) containing 10% (MDA-MB-231, 15%) fetal calf serum, 120 IU/mL penicillin, and 120 μg/mL streptomycin. The cells were grown to 80% confluency before using them for the appropriate assays.

MTT Cell Viability Assay. The rate of cell survival under the action of test substances was evaluated by an improved MTT assay as previously described.[24] The assay is based on the ability of viable cells to metabolize yellow 3-(4,5-dimethylthiazol-2-yl)-2,5-diphenyltetrazolium bromide (MTT, Applichem, Germany) to violet formazan that can be detected spectrophotometrically. In brief, A2780, Cal27, Kyse510, and MDA-MB-231 cell lines were seeded at a density of 5000, 7000, 8000, and 10 000 cells/well in 96-well plates (Corning, Germany). After 24 h, cells were exposed to increased concentrations of the test compounds. Incubation was ended after 72 h, and cell survival was determined by addition of MTT solution (5 mg/mL in phosphate buffered saline). The formazan precipitate was dissolved in DMSO (VWR, Germany). Absorbance was measured at 544 and 690 nm in a FLUOstar microplate reader (BMG LabTech, Offenburg, Germany).

Combination Experiments. For the investigation of the effect of **19i** or vorinostat on the cisplatin induced cytotoxicity, **19i** or vorinostat was added 48 h before cisplatin. After 72 h, the cytotoxic effect was determined with a MTT cell viability assay.

Whole-Cell HDAC Inhibition Assay. The cellular HDAC assay was based on an assay published by Ciossek et al.[25] and Bonfils et al.[26] with minor modifications.

Briefly, human cancer cell lines Cal27sens/Cal27 CisR, Kyse510-sens/Kyse510 CisR, A2780/A2780 CisR, and MDA-MB231sens/CisR were seeded in 96-well tissue culture plates (Corning, Germany) at a density of 1.5 × 10^4 cells/well in a total volume of 90 μL of culture medium. After 24 h, cells were incubated for 18 h with increasing concentrations of test compounds. The reaction was started by adding 10 μL of 3 mM Boc-Lys(ε-Ac)-AMC (Bachem, Germany) to reach a final concentration of 0.3 mM. The cells were incubated with the Boc-Lys(ε-Ac)-AMC for 3 h under cell culture conditions. After this incubation, 100 μL/well stop solution (25 mM Tris-HCl (pH 8), 137 mM NaCl, 2.7 mM KCl, 1 mM $MgCl_2$, 1% NP40, 2.0 mg/mL trypsin, 10 μM vorinostat) was added and the mixture was developed for 3 h under cell culture conditions. Fluorescence intensity was measured at an excitation of 320 nm and emission of 520 nm in a NOVOstar microplate reader (BMG LabTech, Offenburg, Germany).

HDAC IC_{50} Profiling. The in vitro inhibitory activity of compounds **19e**, **19h**, and **19i** against seven human HDAC isoforms (1, 2, 4 C2A, 5 C2A, 6, 8, and 11) were performed at Reaction Biology Corp. (Malvern, PA) with a fluorescent based assay according to the company's standard operating procedure. The IC_{50} values were determined using 10 different concentrations with 3-fold serial dilution starting at 10 μM. TSA and vorinostat were used as reference compounds.

Combination Index Analysis. The combined effect of cisplatin and **19i** or cisplatin and vorinostat was analyzed using the MTT assay. Cell viability was determined from each well relative to the average absorbance of control wells. The combination indexes (CIs) were calculated using CalcuSyn 2.1 software (Biosoft, Cambridge, U.K.) based on the Chou−Talalay method.[27] CI > 1 indicates antagonism. CI = 1 indicates an additive effect, and CI < 1 indicates synergism.

Data Analysis. Concentration−effect curves were constructed with Prism 4.0 (GraphPad, San Diego, CA) by fitting the pooled data of at least three experiments performed in triplicate to the four-parameter logistic equation.

3. Docking Studies. The coordinates of the protein structures were retrieved from the Protein Data Bank (PDB). For cross-docking, the HDAC4 and HDAC8 structures were superimposed based on their C_α atoms. In all cases, all water molecules were removed as were all ions except for the catalytic zinc ion. In the case of multiple protein chains in the PDB file, only the first one was retained. Ligand coordinates were either extracted from the PDB files (for the cross-docking) or generated by Moloc[28] (**19i**). Sybyl atom types were manually assigned to all ligands. The ligands were further prepared by autotors for assigning rotatable bonds. As a docking engine, AutoDock3.0.5[14] was used together with the distance-dependent pair potentials of DrugScore[15a] as an objective function as described in ref 15b. The grids were dimensioned sufficiently large to extend at least 7 Å beyond any atom of the ligands used for cross-docking in their crystallographic binding modes. The same grids were then used for docking **19i**.

Docking was performed using the Lamarkian genetic algorithm. Each docking experiment was repeated 100 times, yielding 100 docked protein−ligand configurations. The following parameters were used for docking: a population size of 100, a random starting position and conformation, a maximal effect of mutation of 2 Å for translation and 50° for rotation, a mutation rate of 0.02, and a crossover rate of 0.80. All docking simulations were performed with a maximum of 50 000 generations. The number of energy evaluations was set to 1.0 × 10^6. Finally, all docked conformations were clustered using a tolerance of 1.0 Å rmsd.

For the cross-docking, the docking accuracy was evaluated by calculating the rmsd between docked ligand poses and the crystallographic binding modes. The ligand pose found on the first scoring

dx.doi.org/10.1021/jm301254q | J. Med. Chem. 2013, 56, 427−436

rank of the largest or second largest cluster was chosen for this. For docking of **19i**, the first pose of the largest or second largest cluster was chosen that showed a distance between the hydroxyl oxygen and the zinc ion below 3 Å. These poses are depicted in Figure 3.

■ ASSOCIATED CONTENT

Supporting Information

Experimental procedures and compound characterization data for all intermediates and target compounds. This material is available free of charge via the Internet at http://pubs.acs.org.

■ AUTHOR INFORMATION

Corresponding Author

*Phone: (+49) 21181-14985. Fax: (+49) 21181-13847. E-mail: thomas.kurz@uni-duesseldorf.de.

Author Contributions

†Linda Marek and Alexandra Hamacher contributed equally to this publication.

Notes

The authors declare no competing financial interest.

■ ACKNOWLEDGMENTS

The Deutsche Forschungsgemeinschaft (DFG) is acknowledged for funds used to purchase the UHR-TOF maXis 4G, Bruker Daltonics HRMS instrument used in this research.

■ DEDICATION

Dedicated to Linda Marek, in memoriam.

■ ABBREVIATIONS USED

CDT, 1,1′-carbonyldi(1,2,4-triazole); CisR, cisplatin resistant subclone; DMAP, 4-dimethylaminopyridine; EDC, 1-ethyl-3-(3-dimethylaminopropyl)carbodiimide hydrochloride; Et_3N, triethylamine; HDAC, histone deacetylase; $HDAC_i$, histone deacetylase inhibitor; HSP90, heat shock protein 90; MTT, 3-(4,5-dimethylthiazol-2-yl)-2,5-diphenyltetrazolium bromide; Pd/C, palladium on activated carbon; rt, room temperature; SAHA, suberoylanilide hydroxamic acid; sens, parental cell line of the CisR subclone; THF, tetrahydrofuran; TSA, trichostatin A

■ REFERENCES

(1) Biel, M.; Wascholowski, V.; Giannis, A. Epigenetics—an epicenter of gene regulation: histones and histone-modifying enzymes. *Angew. Chem., Int. Ed.* **2005**, *44*, 3186−3216.

(2) (a) Paris, M.; Porcelloni, M.; Binaschi, M.; Fattori, D. Histone deacetylase inhibitors: from bench to clinic. *J. Med. Chem.* **2008**, *51*, 1505−1529. (b) Schemies, J.; Sippl, W.; Jung, M. Histone deacetylase inhibitors that target tubulin. *Cancer lett.* **2009**, *280*, 222−232.

(3) Bertrand, P. Inside HDAC with HDAC inhibitors. *Eur. J. Med. Chem.* **2010**, *45*, 2095−2116.

(4) Witt, O.; Deubzer, H. E.; Milde, T.; Oehme, I. HDAC family: What are the cancer relevant targets? *Cancer Lett.* **2009**, *277*, 8−21.

(5) (a) Agis-Balboa, R. C.; Pavelka, Z.; Kerimoglu, C.; Fischer, A. Loss of HDAC5 impairs memory function: implications for Alzheimer's disease. *J. Alzheimer's Dis.* **2013**, *33*, 35−44. (b) Zhang, H.; Xiao, Y.; Zhu, Z.; Li, B.; Greene, M. I. Immune regulation by histone deacetylases: a focus on the alteration of FOXP3 activity. *Immunol. Cell. Biol.* **2012**, *90*, 95−100. (c) Khan, O.; La Thangue, N. B. HDAC inhibitors in cancer biology: emerging mechanisms and clinical applications. *Immunol. Cell Biol.* **2012**, *90*, 85−94.

(6) (a) Miller, T. A.; Witter, D. J.; Belvedere, S. Histone deacetylase inhibitors. *J. Med. Chem.* **2003**, *46*, 5097−5116. (b) Schlimme, S.; Hauser, A.-T.; Carafa, V.; Heinke, R.; Kannan, S.; Stolfa, D. A.; Cellamare, S.; Carotti, A.; Altucci, L.; Jung, M.; Sippl, W. Carbamate prodrug concept for hydroxamate HDAC inhibitors. *ChemMedChem* **2011**, *6*, 1193−1198. (c) Schäfer, S.; Saunders, L.; Schlimme, S.; Valkov, V.; Wagner, J. M.; Kratz, F.; Sippl, W.; Verdin, E.; Jung, M. Pyridylalanine-containing hydroxamic acids as selective HDAC6 inhibitors. *ChemMedChem* **2009**, *4*, 283−290. (d) Stolfa, D. A; Stefanachi, A.; Gajer, J. M.; Nebbioso, A.; Altucci, L.; Cellamare, S.; Jung, M.; Carotti, A. Design, synthesis, and biological evaluation of 2-aminobenzanilide derivatives as potent and selective HDAC inhibitors. *ChemMedChem* **2012**, *7*, 1256−1266.

(7) (a) Finnin, M. S.; Donigian, J. R.; Cohen, A.; Richon, V. M.; Rifkind, R. A.; Marks, P. A.; Breslow, R.; Pavletich, N. P. Structures of a histone deacetylase homologue bound to the TSA and SAHA inhibitors. *Nature* **1999**, *401*, 188−193. (b) Vannini, A.; Volpari, C.; Filocamo, G.; Casavola, E. C.; Brunetti, M.; Renzoni, D.; Chakravarty, P.; Paolini, C.; De Francesco, R.; Gallinari, P.; Steinkühler, C.; Di Marco, S. Crystal structure of a eukaryotic zinc-dependent histone deacetylase, human HDAC8, complexed with a hydroxamic acid inhibitor. *Proc. Natl. Acad. Sci. U.S.A.* **2004**, *101*, 15064−15069. (c) Vannini, A.; Volpari, C.; Gallinari, P.; Jones, P.; Mattu, M.; Carfí, A.; De Francesco, R.; Steinkühler, C.; Di Marco, S. Substrate binding to histone deacetylases as shown by the crystal structure of the HDAC8-substrate complex. *EMBO Rep.* **2007**, *8*, 879−884.

(8) Balasubramanian, S.; Verner, E.; Buggy, J. J. Isoform-specific histone deacetylase inhibitors: the next step? *Cancer Lett.* **2009**, *280*, 211−221.

(9) Thurn, K. T.; Thomas, S.; Moore, A.; Munster, P. N. Rational therapeutic combinations with histone deacetylase inhibitors for the treatment of cancer. *Future Oncol.* **2011**, *7*, 263−283.

(10) Noureen, N.; Rashid, H.; Kalsoom, S. Identification of type-specific anticancer histone deacetylase inhibitors: road to success. *Cancer Chemother. Pharmacol.* **2010**, *66*, 625−633.

(11) Bieliauskas, A. V.; Pflum, M. K. H. Isoform-selective histone deacetylase inhibitors. *Chem. Soc. Rev.* **2008**, *37*, 1402−1413.

(12) Bots, M.; Johnstone, R. W. Rational combinations using HDAC inhibitors. *Clin. Cancer Res.* **2009**, *15*, 3970−3977.

(13) Ong, P.-S.; Wang, X.-Q.; Lin, H.-S.; Chan, S.-Y.; Ho, P. C. Synergistic effects of suberoylanilide hydroxamic acid combined with cisplatin causing cell cycle arrest independent apoptosis in platinum-resistant ovarian cancer cells. *Int. J. Oncol.* **2012**, *40*, 1705−1713.

(14) Morris, G.; Goodsell, D. Automated docking using a Lamarckian genetic algorithm and an empirical binding free energy function. *J. Comput. Chem.* **1998**, *19*, 1639−1662.

(15) (a) Gohlke, H.; Hendlich, M.; Klebe, G. Knowledge-based scoring function to predict protein−ligand interactions. *J. Mol. Biol.* **2000**, *295*, 337−356. (b) Sotriffer, C. A.; Gohlke, H.; Klebe, G. Docking into knowledge-based potential fields: a comparative evaluation of DrugScore. *J. Med. Chem.* **2002**, *45*, 1967−1970.

(16) Bottomley, M. J.; Lo Surdo, P.; Di Giovine, P.; Cirillo, A.; Scarpelli, R.; Ferrigno, F.; Jones, P.; Neddermann, P.; De Francesco, R.; Steinkühler, C.; Gallinari, P.; Carfí, A. Structural and functional analysis of the human HDAC4 catalytic domain reveals a regulatory structural zinc-binding domain. *J. Biol. Chem.* **2008**, *283*, 26694−26704.

(17) (a) Oger, F.; Lecorgne, A.; Sala, E.; Nardese, V.; Demay, F.; Chevance, S.; Desravines, D. C.; Aleksandrova, N.; Le Guével, R.; Lorenzi, S.; Beccari, A. R.; Barath, P.; Hart, D. J.; Bondon, A.; Carettoni, D.; Simonneaux, G.; Salbert, G. Biological and biophysical properties of the histone deacetylase inhibitor suberoylanilide hydroxamic acid are affected by the presence of short alkyl groups on the phenyl ring. *J. Med. Chem.* **2010**, *53*, 1937−1950. (b) Brunsteiner, M.; Petukhov, P. A. Insights from comprehensive multiple receptor docking to HDAC8. *J. Mol. Model.* **2012**, *18*, 3927−3939.

(18) Kazemi, S.; Krüger, D. M.; Sirockin, F.; Gohlke, H. Elastic potential grids: accurate and efficient representation of intermolecular interactions for fully flexible docking. *ChemMedChem* **2009**, *4*, 1264−1268.

(19) Stronach, E. A.; Alfraidi, A.; Rama, N.; Datler, C.; Studd, J.; Agarwal, R.; Guney, T. G.; Gourley, C.; Hennessy, B. T.; Mills, G. B.; Mai, A.; Brown, R.; Dina, R.; Gabra, H. HDAC4-regulated STAT1 activation mediates platinum resistance in ovarian cancer. *Cancer Res.* **2011**, *71*, 4412−4422.
(20) (a) Hager, K.; Franz, A.; Hirsch, A. Self-assembly of chiral depsipeptide dendrimers. *Chem.—Eur. J.* **2006**, *12*, 2663−2679. (b) Li, J.; Yao, S. Q. "Singapore Green": a new fluorescent dye for microarray and bioimaging applications. *Org. Lett.* **2009**, *11*, 405−408.
(21) Gediya, L. K.; Chopra, P.; Purushottamachar, P.; Maheshwari, N.; Njar, V. C. O. A new simple and high-yield synthesis of suberoylanilide hydroxamic acid and its inhibitory effect alone or in combination with retinoids on proliferation of human prostate cancer cells. *J. Med. Chem.* **2005**, *48*, 5047−5051.
(22) Gosepath, E. M.; Eckstein, N.; Hamacher, A.; Servan, K.; von Jonquieres, G.; Lage, H.; Györffy, B.; Royer, H. D.; Kassack, M. U. Acquired cisplatin resistance in the head−neck cancer cell line Cal27 is associated with decreased DKK1 expression and can partially be reversed by overexpression of DKK1. *Int. J. Cancer* **2008**, *123*, 2013−2019.
(23) Eckstein, N.; Servan, K.; Girard, L.; Cai, D.; von Jonquieres, G.; Jaehde, U.; Kassack, M. U.; Gazdar, A. F.; Minna, J. D.; Royer, H. D. Epidermal growth factor receptor pathway analysis identifies amphiregulin as a key factor for cisplatin resistance of human breast cancer cells. *J. Biol. Chem.* **2008**, *283*, 739−750.
(24) Mueller, H.; Kassack, M. U.; Wiese, M. Comparison of the usefulness of the MTT, ATP, and calcein assays to predict the potency of cytotoxic agents in various human cancer cell lines. *J. Biomol. Screening* **2004**, *9*, 506−515.
(25) Ciossek, T.; Julius, H.; Wieland, H.; Maier, T.; Beckers, T. A homogeneous cellular histone deacetylase assay suitable for compound profiling and robotic screening. *Anal. Biochem.* **2008**, *372*, 72−81.
(26) Bonfils, C.; Kalita, A.; Dubay, M.; Siu, L. L.; Carducci, M. A.; Reid, G.; Martell, R. E.; Besterman, J. M.; Li, Z. Evaluation of the pharmacodynamic effects of MGCD0103 from preclinical models to human using a novel HDAC enzyme assay. *Clin. Cancer Res.* **2008**, *14*, 3441−3449.
(27) Chou, T. C. Drug combination studies and their synergy quantification using the Chou−Talalay method. *Cancer Res.* **2010**, *70*, 440−446.
(28) Gerber, P. R.; Müller, K. MAB, a generally applicable molecular force field for structure modelling in medicinal chemistry. *J. Comput.-Aided Mol. Des.* **1995**, *9*, 251−268.